Received: 11 October 2019 | Revised: 28 January 2020 | Accepted: 3 February 2020

DOI: 10.1002/ardp.201900296

FULL PAPER

DPhG ARCH PHARM Archiv der Pharmazie

Novel pyrazolo[3,4-*d*]pyrimidine derivatives inhibit human cancer cell proliferation and induce apoptosis by ROS generation

Supreet Gaonkar[1] | Mohammed Azharuddin Savanur[2] | AfraQuasar A. Nadaf[1] | Mahesh S. Najare[1] | Shivaraj Mantur[1] | Manjunatha Garbhagudi[1] | Sikandar I. Mulla[3] | Imtiyaz Ahmed M. Khazi[1]

[1]Department of Studies in Chemistry, Karnatak University, Dharwad, Karnataka, India

[2]Department of Biochemistry, Indian Institute of Science, Bangalore, Karnataka, India

[3]Department of Biochemistry, School of Applied Sciences, REVA University, Bangalore, Karnataka, India

Correspondence
Mohammed Azharuddin Savanur, Department of Biochemistry, Indian Institute of Science, Bangalore 560012, India.
Email: azharuddinsavanur1985@gmail.com

Imtiyaz Ahmed M. Khazi, Department of Studies in Chemistry, Karnatak University, Dharwad, Karnataka 580003, India.
Email: drimkorgchem@gmail.com

Abstract

The paucity of effective anticancer drugs for successful treatment is a major concern, indicating the strong need for novel therapeutic compounds. In the quest of new molecules, the present study aimed to explore the potential of pyrazolo[3,4-*d*]pyrimidine derivatives as antiproliferative agents. In vitro anticancer screening of selected compounds was done by the National Cancer Institute's Developmental Therapeutics Programme against a panel of 60 cancer cell lines. The lead compound **PP-31d** considerably inhibited the growth of cancer cells, such as NCI-H460 (non-small-cell lung cancer), OVCAR-4 (ovarian cancer), 786-0 (renal cancer), A549 (non-small-cell lung cancer), and ACHN (renal cancer), showing strong anticancer potential, among other derivatives. Kinetic studies of **PP-31d** on NCI-H460 cells revealed a dose-dependent effect with an IC_{50} of 2 μM. The observed inhibition by **PP-31d** is attributed to the generation of reactive oxygen species and the subsequent induction of cellular apoptosis, as evidenced by the increase in the hypodiploid (subG1) population, the early apoptotic cell population, and caspase-3/7 activity, the loss of the mitochondrial membrane potential, and the degradation of nuclear DNA. Collectively, our results demonstrated that pyrazolo[3,4-*d*]pyrimidine derivatives inhibit cancer cell proliferation by inducing apoptosis and, thus, have the potential to be further explored for anticancer properties.

KEYWORDS

antiproliferative, apoptosis, cytotoxic, pyrazolo[3,4-*d*]pyrimidine

1 | INTRODUCTION

Chemotherapy is a systemic treatment to combat uncontrolled proliferation and invasion of cells using bioactive small molecules. It is one of the major therapeutic strategies adopted worldwide for the treatment of different types of cancer. Chemotherapy, either alone or in conjunction with surgery and/or radiotherapy with proper diagnosis, is a prerequisite for adequate and effective cancer treatment. Developing improved combinations of different cytotoxic agents has resulted in clinically relevant molecules helpful in curing cancer patients. However, despite all innovations to increase chemotherapy efficacy, there are limitations associated, such as side effects, multidrug resistance of the

These authors contributed equally to this work.
Supreet Gaonkar and Mohammed A. Savanur contributed equally to this study.

tumor, and limited scope of activity of the available anticancer agents, making it more challenging for the design and synthesis of novel potent drugs with less side effects and a broad spectrum of activity. Therefore, the search for alternative new therapeutic drugs is always in demand.

Pyrimidine and its fused analogs have attracted the interest of medicinal chemists because of their wide range of biological properties. Among the fused pyrimidines, pyrazolopyrimidine is an important scaffold present in many biologically active compounds. As pyrazolopyrimidines have a structural resemblance with purines, they are considered to be biologically active isomeric purine analogs. Many biologically active compounds containing the pyrazolopyrimidine core have been approved by the Food and Drug Administration (Figure 1).

Pyrazolo[3,4-*d*]pyrimidines are important pharmacophores that have shown a broad range of biological potentials, such as antimicrobial,[1] anti-inflammatory,[2] antiviral,[3] anticancer,[4] and antitubercular activities,[5], and so forth. In recent years, the pyrazolo[3,4-*d*]pyrimidine ring system has been an important pharmacophore in anticancer drug discovery.[6–8] There are numerous reports on pyrazolo[3,4-*d*]pyrimidines as selective and potent inhibitors of many kinases, which play a vital role in cancer cell proliferation.[9–13]

In the present study, we report the synthesis and antiproliferative activity of pyrazolo[3,4-*d*]pyrimidine derivatives against a panel of cancer cell lines. This report also explains the mechanism of induced cell death by generation of reactive oxygen species (ROS) and subsequent induction of cellular apoptosis.

2 | RESULTS AND DISCUSSION

2.1 | Chemistry

The synthesis of pyrazolo[3,4-*d*]pyrimidine derivatives (**PP-31a–PP-31d**, **PP-32a–PP-32d**, and **PP-33a–PP-33d**) is outlined in Scheme 1. 2-(1-Ethoxyethylidene)malononitrile (**P1**) was synthesised by reacting 1,1,1-triethoxyethane and malononitrile in acetic anhydride at 110°C for 4 hr. The cyclocondensation of **P1** with 4-bromophenylhydrazinehydrochloride in ethanol in the presence of triethylamine at room temperature for 2 hr yielded the compound 5-amino-1-(4-bromophenyl)-3-methyl-1*H*-pyrazole-4-carbonitrile (**P-2**). The key intermediates (**P-31–P-33**) were synthesised by Suzuki cross-coupling reaction of **P-2** with 4-(trifluoromethoxy)phenylboronic acid, phenylboronic acid, and 4-ethylphenylboronic acid, respectively. Reaction of **P-31–P-33** with formic acid, formamide, benzonitrile, and phenylacetonitrile in different physical and chemical environment yields the desired products **PP-31a–PP-33a**, **PP-31b–PP-33b**, **PP-31c–PP-33c**, and **PP-31d–PP-33d**, respectively. The structures of the synthesised compounds were characterized by infrared (IR), ^{1}H nuclear magnetic resonance (NMR), ^{13}C NMR, single-crystal X-ray diffraction (SC-XRD), and mass spectral analysis. The IR band due to CN stretching at 2,218 cm^{-1} and NH_2 stretching at 3,232 and 3,344 cm^{-1} supports the formation of the structure **P-31**. A singlet at δ 2.32 ppm due to the CH_3 group, a broad singlet at δ 4.74 ppm (parts per million) corresponding to the NH_2 group, and four characteristic doublets of biphenyl at δ 7.31, 7.56, 7.60, and 7.68 ppm confirm the structure of **P-31**. Further, the structure of the intermediate compound **P-31** was confirmed by mass spectral analysis. The structure of one of the intermediate compounds, **P-33** was confirmed by single-crystal X-ray analysis. A broad singlet at δ 12.35 ppm due to amide NH and a characteristic singlet at δ 8.12 ppm corresponding to C6–H of pyrimidine support the formation of the final compound **PP-31a**, which was further confirmed by the liquid chromatography-mass spectrometry (LCMS) data. The ^{1}H NMR spectrum of compound **PP-31d** shows a characteristic singlet at δ 4.06 ppm for two protons corresponding to the bridging CH_2 group, which support the formation of compound. Further, the structure of **PP-31d** was confirmed by ^{13}C NMR and DEPT-135 spectral analysis.

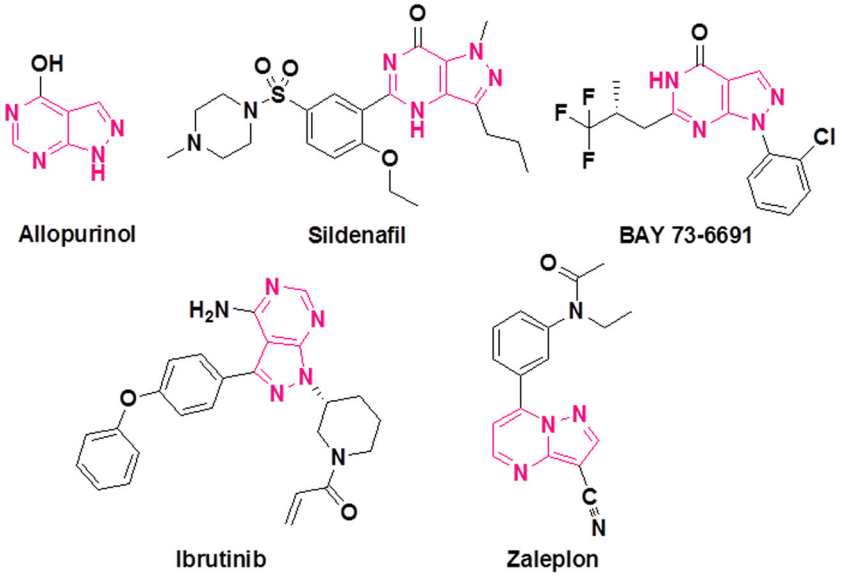

FIGURE 1 Clinically approved drugs containing the pyrazolopyrimidine ring

SCHEME 1 Synthesis of the pyrazolo[3,4-*d*] pyrimidine derivatives

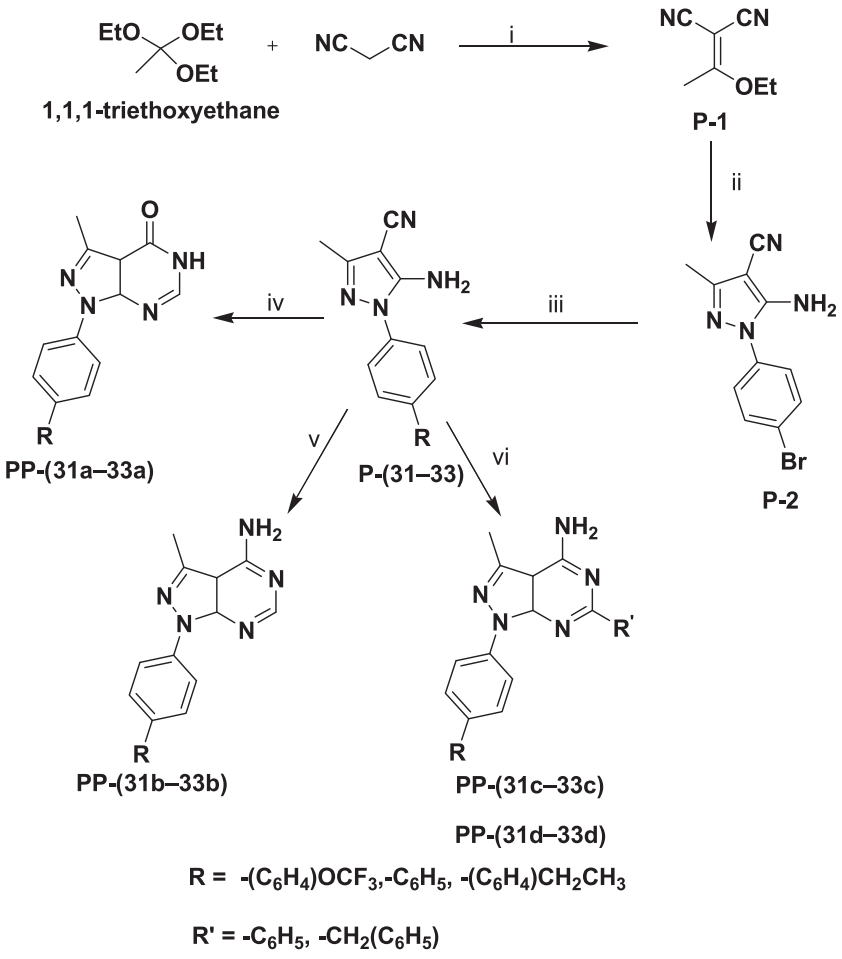

2.2 | Single-crystal X-ray analysis

Single crystals of compound **P-33** were developed by slow evaporation method using acetonitrile as a solvent. A suitable single crystal was collected through the polarizing microscope and then mounted on the Bruker APEX-II CCD diffractometer system, which is equipped with a CCD (charge-coupled device) area detector and a microfocus sealed tube molybdenum source. The crystal was kept at 298 K (2) during the data collection with a scan width of 0.5 mm and a distance of 45 mm from the crystal to the detector. The structure (Figure 2) was solved using the Olex2 with the XT,[14] using Intrinsic Phasing, and refined with the ShelXL refinement package using Least Squares minimization.[15] The presence in the crystal structure of a strong bond CN...N (3.088 Å), short contact interaction between NH...N (2.504 Å), NH...N (2.261 Å), and also CH... π (2.893 Å) make the molecule more stable (Figure 3). Crystal data are listed in Table 1.

2.3 | In vitro anticancer activity

To determine the cytotoxic effect of the synthesised compounds, we deposited the structure of all final compounds in the National Cancer Institute's Developmental Therapeutics Program (Supplementary Information). Among all, seven compounds (**PP-31a**, **PP-31b**, **PP-31c**, **PP-31d**, **PP-32b**, **PP-33a**, and **PP-33d**) have been

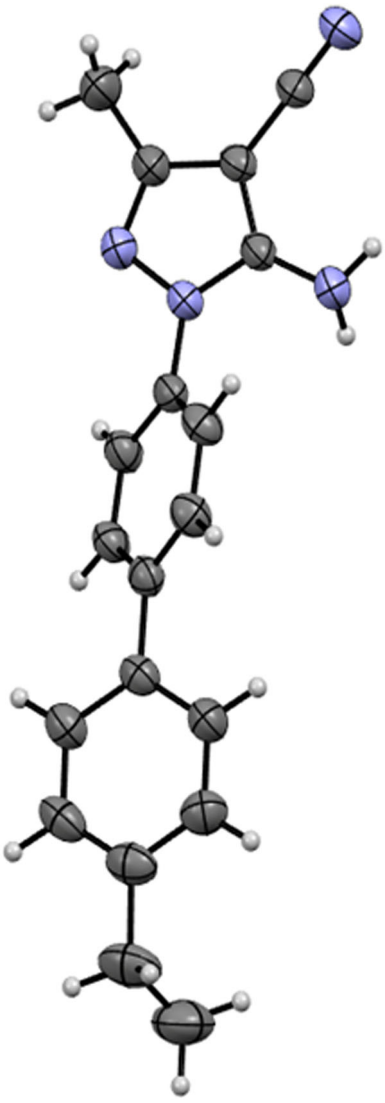

FIGURE 2 ORTEP (Oak Ridge thermal ellipsoid plot) diagram of compound **P-33** with labeling showing 50% displacement ellipsoids (crystal structure drew in Mercury 3.7)

selected for single-dose analysis [10 μM] and tested against 60 human cancer cell lines. Compounds **PP-31d** and **PP-33d** showed good to moderate inhibition against many cancer cell lines. Initial screening results revealed that compounds containing a benzyl group at C-2 of pyrimidine are more potent and showed enhanced cytotoxicity. In particular, compound **PP-31d** showed strong growth inhibition (96.6%) of NCI-H460 cells. Further, we carried out the dose kinetic study of compound **PP-31d** and **PP-33d** on NCI -H460 cells using 3-(4,5-dimethylthiazol-2-yl)-2,5-diphenyl tetrazolium bromide (MTT) assay. The results showed the strong inhibitory activity of compound **PP-31d** on NCI-H460 cells in a dose-dependent manner (Figure 4a). In addition, the growth inhibition effects of these compounds were also tested against human embryonic kidney (HEK293) cells and it was observed that pyrimidine derivatives have a dose-dependent effect with a higher IC_{50} (31.2 μM) value when compared to cancer cells (Figure S2). The effect of compounds **PP-31d** and **PP-33d** on the cellular morphology of NCI-H460 cell was determined. Control cells had a distinct and well-defined morphology, whereas cells treated with compound **PP-31d** and **PP-33d** had indecisive morphology and appeared to be dead (Figure 4b). The cytotoxic effect of **PP-31d** on NCI-H460 cells was evidenced by the morphological changes in the phase-contrast image. The lead compound (**PP-31d**) was further subjected to cell cycle analysis, annexin-V/PI assay, assessment of caspase-3/7 activity, evaluation of mitochondrial membrane potential, and DNA damage studies.

2.3.1 | Compound PP-31d induces accumulation of NCI-H460 cells in the subG1 phase of the cell cycle

Cytotoxic compounds mainly exert their effects by intervening with cell cycle progression, inhibiting cellular proliferation, and thus, inducing cell death.[16–18] The subG1 phase of the cell cycle represents the cells that are hypodiploid and undergoing apoptosis.[19,20] NCI-H460 cells treated with compound **PP-31d** at different concentrations were subjected to cell cycle analysis after propidium iodide (PI) staining to observe the percentage of cells undergoing apoptosis and their distribution in different phases of the cell cycle. The results of the cell cycle analysis of NCI-H460 cells after treatment with compound **PP-31d** are presented in Figure 5a. The DNA content analysis of NCI-H460 cells after **PP-31d** treatment showed a dose-dependent gradual increase in hypodiploid population. Treatment with 10 μM of compound resulted in 28.6%, which increased to 39.2% at 20 μM when compared to 1.8% in control groups, suggesting that **PP-31d** promotes cell death through induction of apoptosis. The percentage distribution of cells in different phases of the cell cycle is represented in bar diagrams (Figure 5b).

2.3.2 | Induction of apoptosis by compound PP-31d

Loss of plasma membrane asymmetry, such as translocation of phosphatidylserine to the outer surface of the plasma membrane, is an early characteristic of apoptosis,[21,22] which can be detected using annexin-V.[23,24] To validate that compound-induced cell death was associated with apoptosis, NCI-H460 cells treated with or without **PP-31d** were analyzed by annexin-V-FITC (fluorescein isothiocyanate)/PI staining, which differentiates viable, early, and late apoptosis or dead cells. Flow cytometry analysis demonstrated a dose-dependent increase in annexin-V stained cells, representing both the early and late apoptotic population. As shown in Figure 6a, a substantial increase in the percentage of early apoptotic cells (49.9%) was observed after **PP-31d** treatment, when compared to the control group (0.5%). Exposure of NCI-H460 cells to higher concentrations of the **PP-31d** resulted in shifting to the late apoptotic stage (annexin-V and PI-positive), indicating that **PP-31d** induces cellular apoptosis in a dose-dependent manner. Figure 6b shows the percentage of NCI-H460 cells in four different quadrants and presents it in the form of bar graphs.

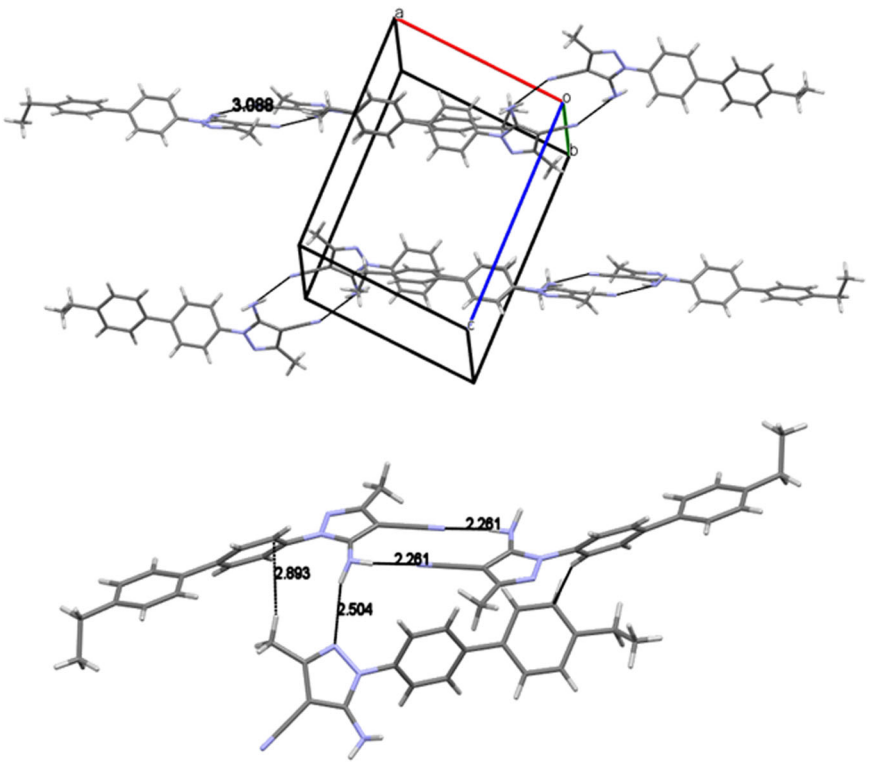

FIGURE 3 Packing diagram of **P-33** with CN…N (3.088 Å), NH…N (2.504 Å), NH…N (2.261 Å) and CH… π (2.893 Å) interactions

2.3.3 | Compound PP-31d attenuates the mitochondrial membrane potential

Increased ROS levels usher disruption of mitochondrial membrane and degeneracy of the electrochemical gradient (loss in mitochondrial membrane potential).[25–27] As **PP-31d**-treated cells showed increased ROS levels, it was important to analyze whether elevated ROS had an impact on mitochondria. Therefore, changes in the mitochondrial membrane potential were analyzed to determine the deleterious effects of ROS on mitochondria. JC-1, a lipophilic cationic dye, was used to determine the effect of **PP-31d** on the mitochondrial membrane potential. JC-1 emits red fluorescence by accumulating in intact mitochondria and is also membrane-potential dependent, which helps in measuring changes in mitochondrial polarization. During apoptosis, mitochondrion depolarizes and mitochondrial membrane potential collapses, leading to accumulation of JC-1 in cytoplasm and emitting green fluorescence.[28] Flow cytometric analysis demonstrated that treatment of NCI-H460 cells with different concentrations of **PP-31d** resulted in depolarization of mitochondrial membrane, as evidenced by the increase in the number of cells positive for green fluorescence (Figure 7a). A remarkable reduction in mitochondrial membrane potential (58.9%) was observed in cells exposed to 20 μM of **PP-31d**, suggesting that the compound-induced cell death involves mitochondrial depolarization-associated apoptosis. Figure 7b shows the percentage of NCI-H460 cells with high and low mitochondrial membrane potential after treatment with and without **PP-31d**. Depolarization of mitochondria after **PP-31d** treatment was also assessed by measuring mitochondrial cytochrome *c* levels and it was observed that the levels of this hemeprotein decreased significantly (Figure S3).

2.3.4 | ROS generation by compound PP-31d

Oxidative damage to biomolecules caused by enhanced ROS levels leads to apoptosis and cell death.[29,30] Thus, cytotoxic compounds that have the ability to enhance ROS levels in cancer cells are potential anticancer agents.[31–33] The ROS-generating ability of **PP-31d** in NCI-H460 cells was determined by 2,7-dichlorodihydro fluorescein diacetate (DCFDA-H2) staining (a nonfluorescent dye emits green fluorescence upon oxidation by ROS) followed by microscopic analysis. Figure 8a shows enhanced green fluorescence, which is a consequence of DCFDA-H2 oxidation due to increased ROS levels upon treatment of cells with **PP-31d**. These results indicate that compound **PP-31d** promotes ROS generation and induces apoptosis in cancer cells.

2.3.5 | Compound PP-31d induces activation of the effector caspase-3/7

The elevated ROS causes oxidative stress and activation of caspases, leading to the induction of apoptosis.[34,35] Activation of effector caspase-3/7 results in DNA condensation and fragmentation, which are characteristic changes associated with the induction of apoptosis.

TABLE 1 Crystal data and structure refinement of compound **P-33**

Identification code	1
Empirical formula	$C_{19}H_{18}N_4$
Formula weight	302.38
Temperature/K	293(2)
Crystal system	monoclinic
Space group	$P2_1/n$
a/Å	11.0142(4)
b/Å	10.0360(3)
c/Å	14.9346(4)
α/°	90
β/°	97.0360(10)
γ/°	90
Volume/Å^3	1,638.42(9)
Z	4
ρ_{calc}/g/cm^3	1.230
μ/mm	0.075
F(000)	644.0
Crystal size/mm^3	0.23 × 0.24 × 0.25
Radiation	MoKα (λ = 0.71073)
2Θ range for data collection/°	4.35 to 49.994
Index ranges	−13 ≤ h ≤ 13, −11 ≤ k ≤ 11, −17 ≤ l ≤ 17
Reflections collected	56,974
Independent reflections	2,853 [R_{int} = 0.0256, R_{sigma} = 0.0087]
Data/restraints/parameters	2853/0/211
Goodness-of-fit on F^2	1.238
Final *R* indexes [$I \geq 2\sigma$ (I)]	R_1 = 0.0451, wR_2 = 0.1489
Final *R* indexes [all data]	R_1 = 0.0589, wR_2 = 0.1729
Largest diff. peak/hole/e Å^{-3}	0.47/−0.52
CCDC number	1526438

Thus, the ability of **PP-31d** to activate effector caspases was determined using appropriate substrates provided in the caspases-3/7 Glo assay kit. Treatment of NCI-H460 cells with **PP-31d** showed a significant increase in caspase-3/7 activity (2.5-fold) as compared to the untreated control, signifying that cell death caused by this compound is linked to the induction of cell apoptosis (Figure 8b).

2.3.6 | Compound PP-31d causes chromatin condensation and DNA fragmentation

Cellular apoptosis is characterized by changes in nuclear morphology, such as nuclear shrinkage, chromatin condensation, and fragmented DNA. Activation of specific endonucleases that cause DNA fragmentation is a known mechanism by which anticancer drugs induce apoptosis in cancer cells.[36] The ability of **PP-31d** to induce changes in nuclear morphology was assessed by determining the condensation of chromatin and DNA fragmentation. Staining of NCI-H460 cells nuclei with 4′,6-diamidino-2-phenylindole (DAPI) after **PP-31d** treatment showed significant chromatin condensation (Figure 8d), indicating the nuclear changes induced by **PP-31d**. Fragmentation of DNA in cells exposed to compound **PP-31d** was determined by agarose gel electrophoresis. Figure 8c shows fragmented DNA and ladder formation after **PP-31d** treatment in a dose-dependent manner, further supporting the evidence that these compounds induced cell death via induction of apoptosis.

3 | CONCLUSION

In summary, a series of 12 pyrazolo[3,4-*d*]pyrimidine derivatives were synthesised and the structure of the compounds was characterized by IR, ^{1}H NMR, ^{13}C NMR, SC-XRD, and mass spectral analysis. Among all, seven compounds (**PP-31a**, **PP-31b**, **PP-31c**, **PP-31d**, **PP-32b**, **PP-33a**, and **PP-33d**) were selected for single-dose analysis against human cancer cell lines. The structure and activity relationship indicates that compounds comprising a benzyl group at C-2 of the pyrimidine are more potent and showed enhanced cytotoxicity. The cell cycle analysis, DNA damage studies, annexin-V/PI assay, evaluation of mitochondrial membrane potential, and assessment of caspase-3/7 activity were carried out to determine the mechanistic details of compound **PP-31d**-induced cancer cell death. These results indicate that the observed anticancer activity of compound **PP-31d** on NCI-H460 cells is due to the induction of apoptosis. Finally, we conclude that pyrazolo[3,4-*d*]pyrimidine derivatives consisting of a benzyl group can be carefully modified further to get more potent anticancer compounds.

4 | EXPERIMENTAL

4.1 | Chemistry

4.1.1 | General

All commercially available solvents and reagents were procured from either Sigma-Aldrich, S D Fine, or Avra Synthesis Ltd. Thin layer chromatographs (TLCs) were run on Merck silica gel 60 F_{254} TLC plates and spots were visualised using ultraviolet light (254 nm) or permanganate staining. Column chromatography was carried out with commercially available silica gel and solvents. All melting points are uncorrected and determined by an open capillary method. NMR spectra were recorded on a 400 MHz Bruker AV 400 spectrometer. Chemical shifts are expressed in ppm relative to the solvent peak. NMR spin multiplicities are assigned as s (singlet),

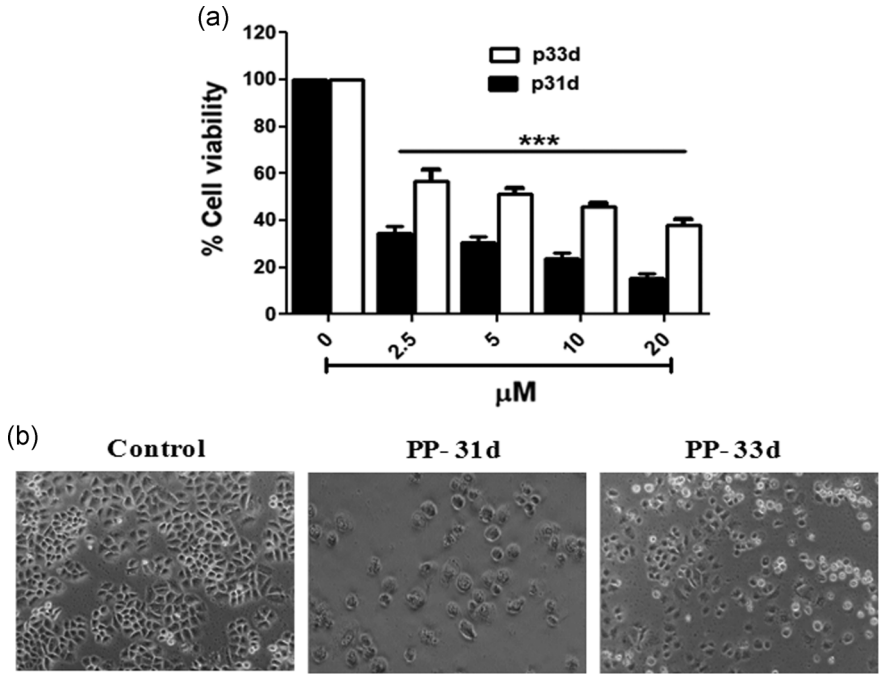

FIGURE 4 Antiproliferative activity of compounds **PP-31d** and **PP-33d** on NCI-H460 cancer cells. Dose-dependent effect of compounds **PP-31d** and **PP-33d** on human lung cancer cell (NCI-H460) proliferation was determined by MTT (3-(4,5-dimethylthiazol-2-yl)-2,5-diphenyl tetrazolium bromide) assay. (a) Graphical representation of percent cell viability at different concentrations (0–20 μM) of **PP-31d** and **PP-33d**, scanning electron microscopy of triplicates from three different experiments is represented by error bars, ***$p > 0.001$. (b) NCI-H460 cell morphology after treatment with or without **PP-31d** and **PP-33d** compounds was analyzed and photographed using a phase-contrast microscope

d (doublet), t (triplet), q (quartet), bs (broad singlet), dd (doublet of doublet), and m (multiplet, for unresolved lines). Coupling constants (*J*) were expressed in hertz (Hz). Mass spectra were recorded using Shimadzu GCMS-QP2010S.

The InChI codes of the investigated compounds together with some biological activity data are provided as Supporting Information.

4.1.2 | General procedure for the synthesis of P-31–P-33

To a mixture of **P-2** (2 g, 7.246 mmol), anhydrous potassium carbonate (2 g, 14.493 mmol) and [1,1′-bis(diphenylphosphino)ferrocene] dichloropalladium(II) dichloromethane complex (0.295 g 0.3623 mmol)

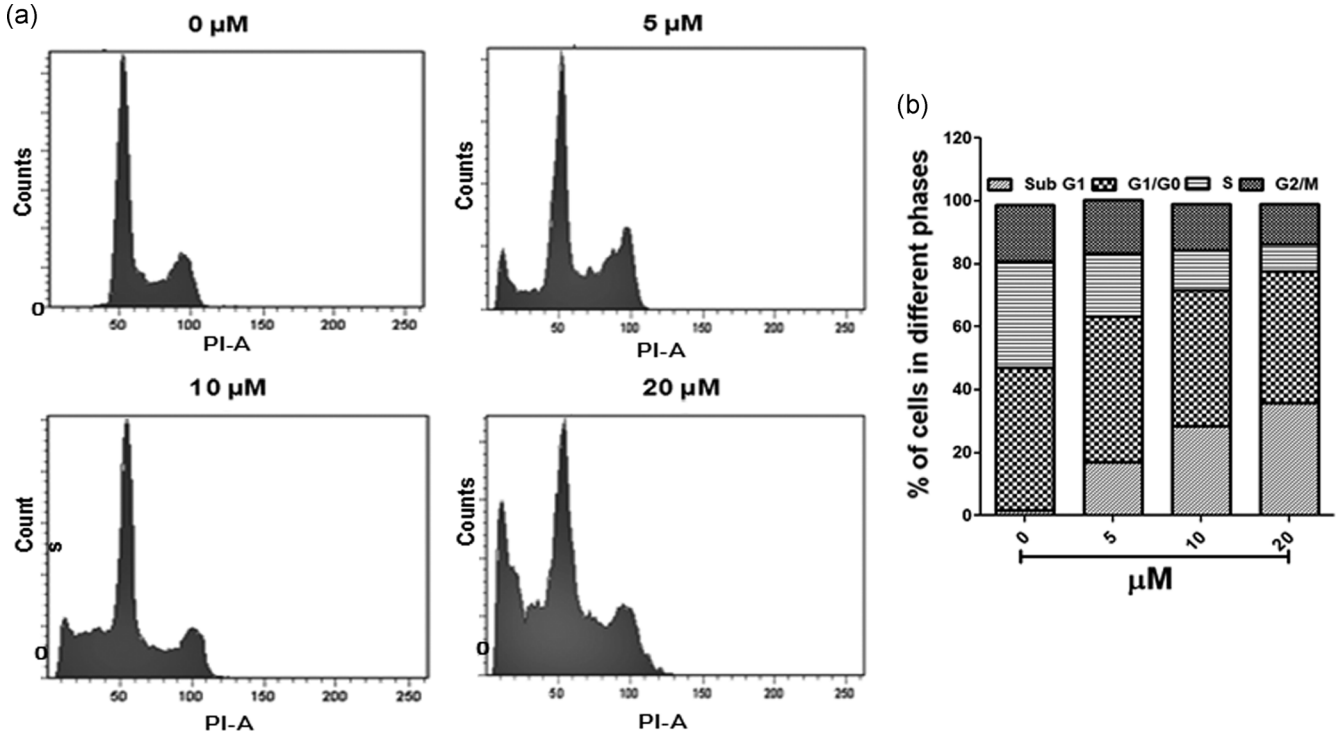

FIGURE 5 Cell cycle analysis of **PP-31d** treated cancer cells. (a) Histograms represent effect of **PP-31d** on distribution of NCI-H460 cells in different phases of cell cycle at different concentrations (0–20 μM). (b) Percentage of NCI-H460 cell population in different phases subG1, G1, S, and G2–M of the cell cycle after treatment with **PP-31d** are represented as a bar graph

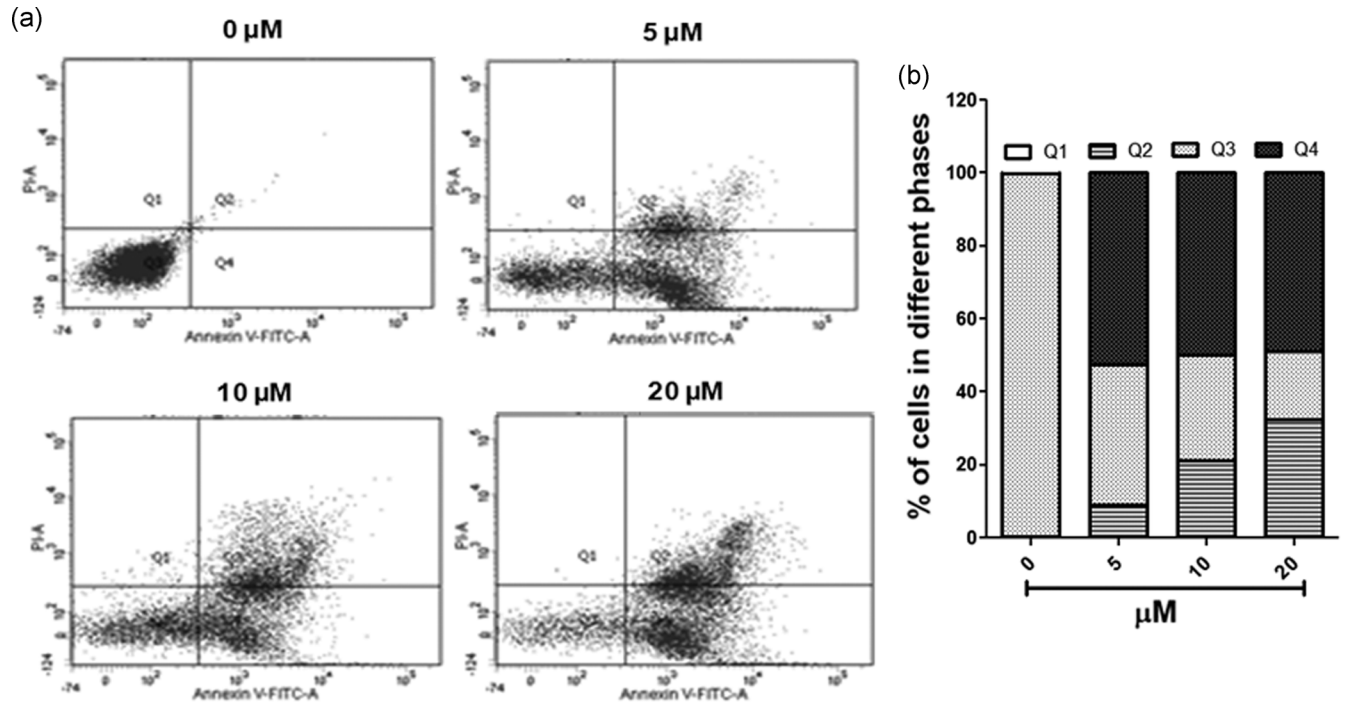

FIGURE 6 Induction of cellular apoptosis by compound **PP-31d**. (a) Histograms represent effect of **PP-31d** on distribution of NCI-H460 cells in different phases Q1 (necrotic/dead cells), Q2 (late apoptosis cells), Q3 (live cells), and Q4 (early apoptosis cells) at different concentrations (0–20 µM). (b) Percentage of NCI-H460 cell population in Q1, Q2, Q3, and Q4 phases after **PP-31d** compound treatment are represented as a bar graph

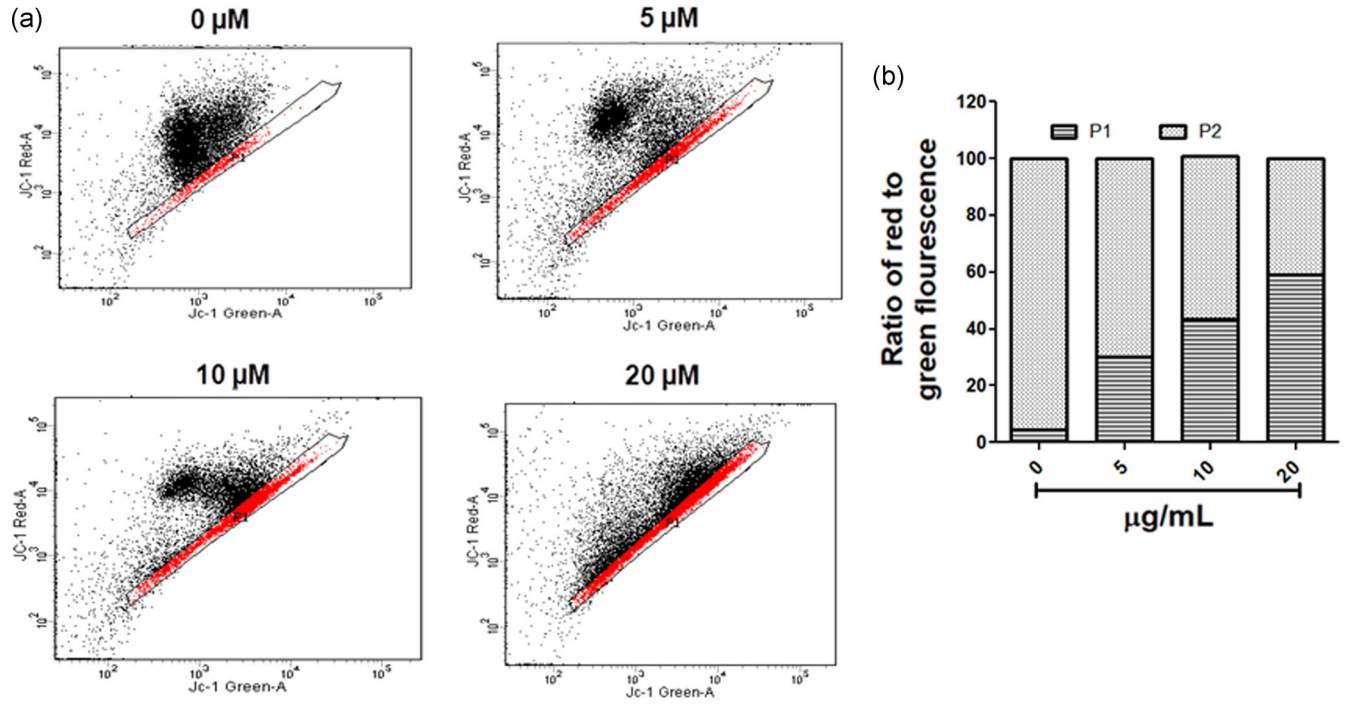

FIGURE 7 **PP-31d** induces depolarization of mitochondria and loss of membrane potential. (a) Density plot depicts effect of **PP-31d** on JC-1-stained NCI-H460 cells at different concentrations (0–20 µM). Cells emitting green fluorescence and with low mitochondrial membrane potential are represented as P1. (b) Percentage of cells emitting red fluorescent and with high mitochondrial membrane potential (P2) against cells emitting green fluorescence and low mitochondrial membrane potential (P1) are represented as a bar graph

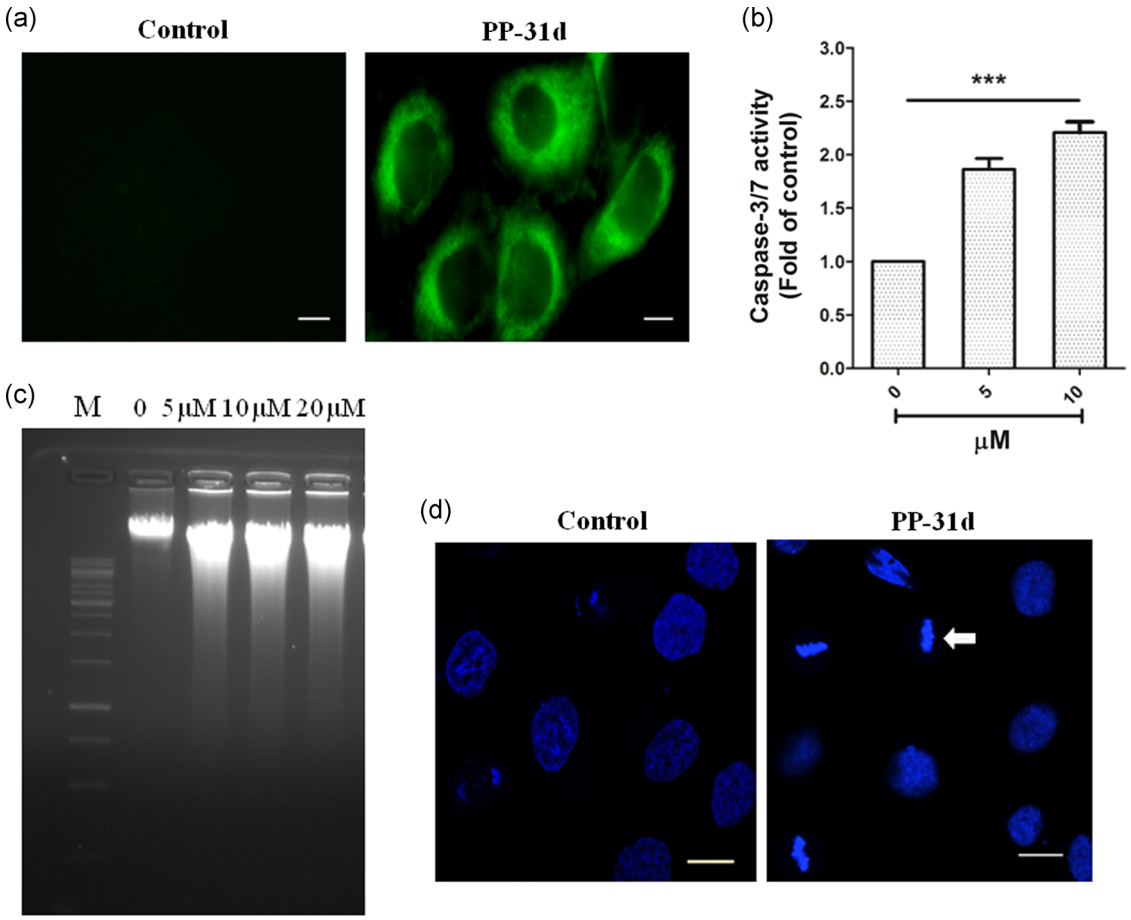

FIGURE 8 Evaluation of **PP-31d** induced apoptotic mechanism: Analysis of ROS production, activation of caspases, chromatin condensation, and DNA fragmentation. (a) Effect of **PP-31d** on intracellular ROS production was determined by fluorescence microscopy using ROS-specific dye DCFDA-H2. (b) Effect of **PP-31d** on activation of caspase-3/7 in NCI-H460 cells was determined by measuring caspase-3/7 activity using caspase-3/7 Glo assay and represented as fold increase in activity, ***$p > 0.001$. (c) Effects of different concentrations (0–20 μM) of **PP-31d** on NCI-H460 cellular DNA are represented by agarose gel profiles. (d) DAPI-staining showing the chromatin-condensed nuclei in apoptotic cells following **PP-31d** treatment. DAPI, 4′,6-diamidino-2-phenylindole; DCFDA, 2,7-dichlorodihydro fluorescein diacetate; M, marker; ROS, reactive oxygen species

in ethanol (20 ml), different phenylboronic acids (7.971 mmol) were added. The reaction mixture was heated at 80°C for 6–8 hr, and the progress of the reaction was observed by TLC. The reaction mixture was cooled, extracted with ethyl acetate, and dried over anhydrous $MgSO_4$. The obtained organic layer was filtered through celite 545 to remove the remaining fine catalyst particles. Solvent was removed under reduced pressure and the crude product obtained was purified by column chromatography to obtain the key intermediates (**P-31–P-33**).

*5-Amino-3-methyl-1-[4′-(trifluoromethoxy)-(1,1′-biphenyl)-4-yl]-1H-pyrazole-4-carbonitrile (**P-31**)*

Light yellow solid (82% yield); mp: 122–124°C; IR (KBr) $\upsilon\,cm^{-1}$: 3,344, 3,232, 2,969, 2,925, 2,218, 1,644, 1,561, 1,535, 1,253, 1,167, 834, and 676; ^1H NMR (400 MHz, $CDCl_3$) δ 7.68 (d, J = 8.6 Hz, 2H), 7.60 (d, J = 8.8 Hz, 2H), 7.56 (d, J = 8.6 Hz, 2H), 7.31 (d, J = 8.0 Hz, 2H), 4.74 (bs, 2H), and 2.32 (s, 3H); ^{13}C NMR (101 MHz, $CDCl_3$) δ ^{13}C NMR (101 MHz, CDCl3) δ 151.27, 150.26, 149.19, 149.17, 140.06, 138.39, 136.55, 129.87, 128.19, 124.42, 121.67, 119.03, 114.51, and 12.93; LCMS: *m/z* 359.

*1-[(1,1′-Biphenyl)-4-yl]-5-amino-3-methyl-1H-pyrazole-4-carbonitrile (**P-32**)*

Light yellow solid (78% yield); mp: 130–134°C; ^1H NMR (400 MHz, $CDCl_3$) δ 7.70 (d, J = 8.2 Hz, 2H), 7.63 (d, J = 8.4 Hz, 2H), 7.54 (d, J = 8.6 Hz, 2H), 7.34 (d, J = 8.1 Hz, 2H), 7.24 (t, J = 7.9 Hz, 1H), 4.70 (bs, 2H), and 2.31 (s, 3H); ^{13}C NMR (101 MHz, $CDCl_3$) δ 152.01, 151.06, 150.29, 149.76, 140.34, 139.08, 138.14, 129.37, 128.65, 127.34, 126.89, 106.38, and 13.01; GCMS: *m/z* 274.

*5-Amino-1-[4′-ethyl-(1,1′-biphenyl)-4-yl]-3-methyl-1H-pyrazole-4-carbonitrile (**P-33**)*

Light green solid (83% yield); mp: 150–152°C; ^1H NMR (400 MHz, $CDCl_3$) δ 7.66 (d, J = 8.0 Hz, 2H), 7.60 (d, J = 8.1 Hz, 2H), 7.57 (d, J = 8.3 Hz, 2H), 7.30 (d, J = 7.8 Hz, 2H), 4.69 (bs, 2H), 2.62 (q, J = 7.8 Hz, 2H), 2.35 (s, 3H) and 1.26 (t, J = 7.6 Hz, 3H); ^{13}C NMR (101 MHz, $CDCl_3$) δ 152.70, 151.67, 150.94, 149.58, 141.03, 140.36, 139.41, 130.88, 129.26, 128.85, 129.18, 104.97, 34.39, 14.65, and 12.94; GCMS: *m/z* 302.

4.1.3 | General procedure for the synthesis of PP-31a–PP-33a

To the intermediates **P-31–P-33** (1 mmol), formic acid (5 ml) was added and refluxed for 6–8 hr. The reaction mixture was cooled and the solid was separated by filtration, washed with excess amount of water, dried, and recrystallized from formic acid to give compounds **PP-31a–PP-33a**.

*3-Methyl-1-[4′-(trifluoromethoxy)-(1,1′-biphenyl)-4-yl]-1,5-dihydro-4*H*-pyrazolo[3,4-*d*]pyrimidin-4-one (**PP-31a**)*

White solid (85% yield); mp: >250°C; ^{1}H NMR (400 MHz, dimethyl sulfoxide [DMSO]-d_6) δ 12.35 (s, 1H), 8.14 (s, 1H), 8.13 (d, J = 5.8 Hz, 2H), 7.83–7.80 (m, 4H), 7.44 (d, J = 8.3 Hz, 2H), and 2.51 (s, 3H); ^{13}C NMR (101 MHz, $CDCl_3$) δ 159.53, 155.19, 151.65, 148.24, 139.36, 137.89, 136.19, 128.41, 127.68, 126.70, 126.06. 124.55, 117.03, 106.39, and 13.36; GCMS: m/z 386.

*1-[(1,1′-Biphenyl)-4-yl]-3-methyl-1,5-dihydro-4*H*-pyrazolo[3,4-*d*]pyrimidin-4-one (**PP-32a**)*

White solid (81% yield); mp: >250°C; ^{1}H NMR (400 MHz, DMSO-d_6) δ 12.38 (s, 1H), 8.17 (s, 1H), 8.15 (d, J = 8.7 Hz, 2H), 7.83 (d, J = 8.7 Hz, 2H), 7.72 (d, J = 7.3 Hz, 2H), 7.50 (t, J = 7.6 Hz, 2H), 7.40 (t, J = 7.3 Hz, 1H), and 2.55 (s, 3H); ^{13}C NMR (101 MHz, $CDCl_3$) δ 157.91, 152.28, 148.91, 146.04, 139.16, 138.11, 137.58, 128.95, 127.58, 127.24, 126.56, 121.45, 105.81, and 13.33; GCMS: m/z 302.

*1-[4′-Ethyl-(1,1′-biphenyl)-4-yl]-3-methyl-1,5-dihydro-4*H*-pyrazolo[3,4-*d*]pyrimidin-4-one (**PP-33a**)*

White solid (87% yield); mp: >250°C; ^{1}H NMR (400 MHz, DMSO-d_6) δ 12.35 (s, 1H), 8.16 (s, 1H), 8.13 (d, J = 8.4 Hz, 2H), 7.85 (d, J = 8.7 Hz, 2H), 7.61 (d, J = 7.3 Hz, 2H), 7.43 (d, J = 8.0 Hz, 2H), 2.65 (q, J = 7.6 Hz, 2H), 2.53 (s, 3H), and 1.25 (t, J = 7.8 Hz, 3H); ^{13}C NMR (101 MHz, $CDCl_3$) δ 158.15, 152.39, 148.82, 147.06, 139.54, 138.11, 137.58, 130.12, 128.75, 126.45, 125.73, 121.97, 106.11, 33.08, 14.94, and 13.31; GCMS: m/z 330.

4.1.4 | General procedure for the synthesis of PP-31b–PP-33b

The intermediates **P-31–P-33** (1 mmol) were refluxed in formamide for 4–6 hr. The reaction mixture was cooled and the precipitate was filtered, dried, and recrystallized from ethanol to afford the desired products **PP-31b–PP-33b**.

*3-Methyl-1-[4′-(trifluoromethoxy)-(1,1′-biphenyl)-4-yl]-1*H*-pyrazolo[3,4-*d*]pyrimidin-4-amine (**PP-31b**)*

White solid (69% yield); mp: 205–207°C; ^{1}H NMR (400 MHz, DMSO-d_6) δ 8.33 (d, J = 8.8 Hz, 2H), 8.31 (s, 1H), 7.85 (d, J = 8.4 Hz, 4H), 7.65–7.31 (m, 4H), and 2.67 (s, 3H); ^{13}C NMR (101 MHz, $CDCl_3$) 158.64, 156.60, 154.36, 147.79, 143.15, 138.68, 138.63, 135.54, 128.35, 127.40, 121.45, 120.38, 118.84, 100.39, and 14.47; GCMS: m/z 385.

*1-[(1,1′-Biphenyl)-4-yl]-3-methyl-1*H*-pyrazolo[3,4-*d*]pyrimidin-4-amine (**PP-32b**)*

White solid (72% yield); mp: 180–182°C; ^{1}H NMR (400 MHz, DMSO-d_6) δ 8.34 (d, J = 8.2 Hz, 2H), 8.31 (s, 1H), 7.85 (d, J = 7.8 Hz, 2H), 7.81 (d, J = 7.6 Hz, 2H), 7.63–7.29 (m, 4H), 7.33 (t, J = 7.4 Hz, 1H), and 2.63 (s, 3H); ^{13}C NMR (101 MHz, $CDCl_3$) 159.47, 156.68, 153.93, 145.87, 139.24, 137.68, 135.54, 131.39, 128.18, 127.77, 121.94, 120.82, 101.06, and 14.69; GCMS: m/z 301.

*1-[4′-Ethyl-(1,1′-biphenyl)-4-yl]-3-methyl-6-phenyl-1*H*-pyrazolo[3,4-*d*]pyrimidin-4-amine (**PP-33b**)*

White solid (68% yield); mp: 197–199°C; ^{1}H NMR (400 MHz, DMSO-d_6) δ 8.35 (d, J = 8.4 Hz, 2H), 8.32 (s, 1H), 7.83 (d, J = 7.8 Hz, 2H), 7.78 (d, J = 8.2 Hz, 2H), 7.66–7.32 (m, 4H), 2.73 (q, J = 7.3 Hz, 2H), 2.61 (s, 3H), and 1.27 (t, J = 7.5 Hz, 3H); ^{13}C NMR (101 MHz, $CDCl_3$) 160.08, 157.38, 152.76, 144.88, 139.56, 138.23, 136.19, 132.06, 128.79, 127.34, 122.68, 121.41, 100.83, 35.49, 14.58, and 12.75; GCMS: m/z 329.

4.1.5 | General procedure for the synthesis of PP-31c–PP-33c and PP-31d–PP-33d

To a suspension of **P-31–P-33** (1 mmol), potassium *tert*-butoxide (0.2 equiv) in *tert*-butanol (5 ml), benzonitrile, or phenylacetonitrile (1.2 equiv) was added and heated at 80°C for 4–6 hr. The reaction mixture was concentrated under vacuum, solid was dissolved in water and neutralized with 1 N HCl. The solid separated from filtration was dried and recrystallized from ethanol to give the desired products **PP-31c–PP-33c** and **PP-31d–PP-33d**.

*3-Methyl-6-phenyl-1-[4′-(trifluoromethoxy)-(1,1′-biphenyl)-4-yl]-1*H*-pyrazolo[3,4-*d*]pyrimidin-4-amine (**PP-31c**)*

White solid (72% yield); mp: 215–218°C; ^{1}H NMR (400 MHz, DMSO-d_6) δ 8.49 (dd, J = 6.7, 3.1 Hz, 2H), 8.46 (d, J = 8.7 Hz, 2H), 7.91–7.87 (m, 4H), 7.66–7.41 (m, 7H), and 2.69 (s, 3H); ^{13}C NMR (101 MHz, $CDCl_3$) δ 161.74, 158.57, 155.64, 147.77, 143.20, 138.83, 138.67, 137.90, 135.35, 133.29, 132.18, 130.39, 129.45, 128.30, 127.44, 121.41, 120.29, 99.29, and 14.49; GCMS: m/z 461.

*1-[(1,1′-Biphenyl)-4-yl]-3-methyl-6-phenyl-1*H*-pyrazolo[3,4-*d*]pyrimidin-4-amine (**PP-32c**)*

White solid (70% yield); mp: 192–194°C; ^{1}H NMR (400 MHz, DMSO-d_6) δ 8.47 (dd, J = 7.2, 3.1 Hz, 2H), 8.43 (d, J = 8.7 Hz, 2H), 7.89–7.83 (m, 4H), 7.63–7.38 (m, 7H), 7.30 (t, J = 7.8 Hz, 1H), and 2.67 (s, 3H); ^{13}C NMR (101 MHz, $CDCl_3$) δ 161.53, 158.49, 154.83, 144.70, 138.21, 137.84, 137.24, 134.70, 132.93, 132.07, 130.37, 129.58, 129.04, 128.76, 127.13, 120.81, 100.14, and 14.50; GCMS: m/z 377.

*1-[4′-Ethyl-(1,1′-biphenyl)-4-yl]-3-methyl-6-phenyl-1*H*-pyrazolo[3,4-*d*]pyrimidin-4-amine (**PP-33c**)*

White solid (69% yield); mp: 197–200°C; ^{1}H NMR (400 MHz, DMSO-d_6) δ 8.46–8.41 (m, 4H), 7.87 (d, J = 8.2, 2H), 7.84 (d, J = 8.1 Hz, 2H), 7.65–7.39 (m, 7H), 2.71 (q, J = 7.1 Hz, 2H), 2.64 (s, 3H), and 1.25

(t, J = 7.4 Hz, 3H); ^{13}C NMR (101 MHz, $CDCl_3$) δ 162.05, 159.16, 154.77, 144.82, 138.30, 137.89, 137.33, 135.09, 132.52, 132.11, 130.65, 129.21, 128.49, 128.09, 127.69, 122.38, 99.83, 35.91, 14.47, and 12.89; GCMS: *m/z* 405.

*6-Benzyl-3-methyl-1-[4-(4-trifluoromethoxyphenyl)phenyl]-1*H*-pyrazolo[3,4-*d*]pyrimidin-4-amine (**PP-31d**)*

White solid (75% yield); mp: 192–194°C; ^{1}H NMR (400 MHz, DMSO-d_6) 8.35 (d, J = 8.7 Hz, 2H), 7.83 (t, J = 9.3 Hz, 4H), 7.68–7.09 (m, 9H), 4.04 (d, J = 13.2 Hz, 2H), and 2.63 (s, 3H). ^{13}C NMR (101 MHz, $CDCl_3$) δ 167.47, 158.64, 155.43, 147.76, 143.03, 138.88, 138.81, 138.69, 135.31, 128.95, 128.30, 128.16, 127.33, 126.09, 121.41, 120.19, 118.85, 98.73, 45.30, and 14.46; GCMS: *m/z* 475.

*1-[(1,1′-Biphenyl)-4-yl]-6-benzyl-3-methyl-1*H*-pyrazolo[3,4-*d*]pyrimidin-4-amine (**PP-32d**)*

White solid (69% yield); mp: 179–182°C; ^{1}H NMR (400 MHz, DMSO-d_6) δ 8.33 (d, J = 8.4 Hz, 2H), 7.81 (d, J = 8.4 Hz, 2H), 7.63 (d, J = 8.0 Hz, 2H), 7.62–7.13 (m, 10H), 4.04 (s, 2H), and 2.60 (s, 3H); ^{13}C NMR (101 MHz, $CDCl_3$) δ 168.15, 158.65, 156.04, 143.98, 139.13, 138.65, 138.02, 136.11, 130.94, 128.43, 127.84, 127.66, 127.32, 126.71, 123.88, 121.90, 99.08, 45.32, and 14.47; GCMS: *m/z* 391.

*6-Benzyl-1-[4′-ethyl-(1,1′-biphenyl)-4-yl]-3-methyl-1*H*-pyrazolo[3,4-*d*]pyrimidin-4-amine (**PP-33d**)*

White solid (74% yield); mp: 185–188°C; ^{1}H NMR (400 MHz, DMSO-d_6) δ 8.31 (d, J = 8.8 Hz, 2H), 7.79 (d, J = 8.8 Hz, 2H), 7.65 (d, J = 8.2 Hz, 2H), 7.62–7.13 (m, 9H), 4.05 (s, 2H), 2.71–2.60 (m, 5H), and 1.23 (t, J = 7.6 Hz, 3H); ^{13}C NMR (101 MHz, $CDCl_3$) δ 167.23, 158.77, 155.69, 143.39, 138.74, 138.61, 138.38, 135.12, 130.94, 128.16, 128.03, 127.89, 127.30, 126.25, 123.85, 121.62, 99.19, 45.28, 35.36, 14.46, and 12.93; GCMS: *m/z* 419.

4.2 | In vitro anticancer activity

4.2.1 | Cell lines and culture conditions

Human large cell lung cancer cell lines (NCI-H460) were purchased from National Center for Cell Science, Pune, India and cultured RPMI-1640 containing 10% fetal bovine serum, 100 µg/ml of penicillin, and 100 µg/ml of streptomycin at 37°C in a humidified atmosphere containing 5% CO_2.

4.2.2 | Assessment of cell viability and morphology

The viability of NCI-H460 cells was analyzed after treatment with compounds **PP-31d** and **PP-33d** using MTT assay. Briefly, cells were seeded at a density of 5×10^4 cells/ml in 96-well plates followed by treatment with different concentrations (2.5, 5, 10, and 20 µM) of compounds for 24 hr. DMSO-treated cells were used as the vehicle control. Further, to each well, 10 µl of MTT (5 mg/ml) solution was added and incubated for 4 hr. Cells were lysed using 10% sodium dodecyl sulfate (100 µl/well) in 0.01 N HCl and absorbance was measured using Tecan i-200 microplate reader at 570 nm, with a reference wavelength of 640 nm. Percent viability was calculated by considering vehicle control as 100%. In another experiment, NCI-H460 cells after treatment with compound **PP-31d** and **PP-33d** as mentioned above were photographed using a phase-contrast microscope to determine changes in cellular morphology.

4.2.3 | Cell cycle analysis

NCI-H460 cells, after treatment with compound **PP-31d**, were subjected to cell cycle analysis, and the distribution of cells in different phases of the cycle was determined by flow cytometry. Briefly, 0.1×10^6 cells were treated with different concentrations (5, 10, and 20 µM) of compounds for 24 hr. After treatment, the cells were harvested by trypsinization, washed with phosphate-buffered saline (PBS), and fixed in 70% chilled ethanol. Rehydration of cells was carried out using PBS and treated with 50 µl ribonuclease A (5 mg/ml in PBS, DNase-free) for 4 hr at 37°C to hydrolyze RNA. The cells were then stained with PI (50 µg/ml in PBS) for 30 min at 37°C, and the DNA content was analyzed on the FL-2A channel of a flow cytometer (FACS Calibur, BD) equipped with a 488 nm argon laser. The data were analyzed by Cell Quest Pro software (BD) for the distribution of cells in different phases of the cell cycle.

4.2.4 | Detection of apoptosis by annexin-V/PI staining

NCI-H460 cells (0.1×10^6) were cultured in 12-well plates and treated with or without compound **PP-31d** for 24 hr. After treatment, cells were harvested, washed, and resuspended in the binding buffer from BD annexin-V kit. Incubation of cell suspension with FITC annexin-V (5 µl) and PI (5 µl) was carried out in the dark for 5 min at 37°C. Cells undergoing apoptosis were then analyzed using flow cytometry (FACS Calibur; BD). The percentages of cells positive for annexin-V, PI alone and both annexin-V and PI were calculated by dot blot analysis using Cell Quest Pro software (BD Biosciences).

4.2.5 | Analysis of the mitochondrial membrane potential

Changes in the mitochondrial membrane potential were determined using lipophilic and cationic dye 5,5′,6,6′-tetrachloro-1,1′,3,3′-tetraethylbenzimidazolylcarbocyanine iodide (JC-1). Compound **PP-31d** was incubated at different concentrations (5, 10, and 20 µM) with NCI-H460 cells (0.1×10^6) for 24 hr. Cells were then harvested by gentle trypsinization, washed with PBS, and resuspended in freshly prepared 1 ml JC-1 (2.5 µM) solution at 37°C for 20 min. The mitochondrial membrane potential of NCI-H460 cells was analyzed

by flow cytometer (FACS Calibur, BD) with an excitation of 488 nm and an emission of 530 nm.

4.2.6 | Detection of intracellular ROS generation

DCFDA-H2, a cell-permeable fluorescent probe, was used to determine intracellular ROS production. Five micrometers of the compound **PP-31d** was incubated with NCI-H460 cells for 24 hr, followed by washing and staining with 15 μM DCFDA-H2 for 10 min at 30°C. The relative fluorescence intensity was analyzed using fluorescence microscopy.

4.2.7 | Determination of caspase-3/7 activity

To determine the potential of compound **PP-31d** to induce apoptosis, caspase-3/7 activity was measured, as per the manufacturer's protocol supplied in the caspase-activity detection kit (Promega). NCI-H460 cells (10×10^4 cells/ml) were treated with compound **PP-31d**, as described previously in cell viability assay, and induction of cellular apoptosis was determined by measuring caspase-3/7 activity using caspase Glo-3/7 assay.

4.2.8 | Nuclear morphological changes

To determine chromatin condensation and changes in the nuclear morphology of NCI-H460 cells treated with **PP-31d**, DAPI, a DNA-specific dye was used. Briefly, compound **PP-31d** was incubated with cells for 24 hr, washed, and fixed with 2% neutral buffered formalin solution for 10 min. 0.2% Triton-X was used to permeablize cells, followed by staining with DAPI (1 mg/ml) for 10 min. Changes in nuclear morphology were examined using a fluorescence microscope.

4.2.9 | DNA fragmentation assay

The nuclear DNA undergoing fragmentation after treatment with compounds was determined using agarose gel electrophoresis. Briefly, different concentrations of **PP-31d** (5, 10, and 20 μM) were incubated with NCI-H460 cells for 24 hr. After treatment, the cells were washed and harvested, and isolation of genomic DNA was carried out using a standard protocol. DNA samples were resolved using agarose gel (2%) electrophoresis to visualise fragmentation of DNA. A standard DNA marker was used to compare the fragmentation.

ACKNOWLEDGMENTS

The authors gratefully acknowledge National Cancer Institute, USA, for the initial anticancer screening under DTP and NCCS Pune, for providing NCI-H460 cells. We are also thankful to the University Scientific Instrumentation Center (USIC), Karnatak University, Dharwad for Spectral Analysis. One of the authors, Supreet Gaonkar, is thankful to UGC, New Delhi, for providing Senior Research Fellowship (SRF).

CONFLICT OF INTERESTS

The authors declare that there are no conflicts of interests.

ORCID

Mohammed Azharuddin Savanur http://orcid.org/0000-0002-8903-2265

Imtiyaz Ahmed M. Khazi http://orcid.org/0000-0001-8216-1913

REFERENCES

[1] H. A. Abd El Razik, A. E. Abdel Wahab, *Arch. Pharm. Chem. Life Sci.* **2011**, *11*, 184.
[2] S. B. Yewale, S. B. Ganorkar, K. G. Baheti, R. U. Shelke, *Bioorg. Med. Chem. Lett.* **2012**, *22*, 6616.
[3] A. E. Rashad, A. H. Shamroukh, R. E. Abdel-Megeid, A. Mostafa, M. A. Ali, K. Banert, *Nucleosides Nucleotides Nucleic Acids* **2010**, *29*, 809.
[4] M. M. Ghorab, F. A. Ragab, S. I. Alqasoumi, A. M. Alafeefy, S. A. Aboulmagd, *Eur. J. Med. Chem.* **2010**, *45*, 171.
[5] A. R. Trivedi, B. H. Dholariya, C. P. Vakhariya, D. K. Dodiya, H. K. Ram, V. B. Kataria, A. B. Siddiqui, V. H. Shah, *Med. Chem. Res.* **2012**, *21*, 1887.
[6] M. M. El-Enany, M. M. Kamel, O. M. Khalil, H. B. El-Nassan, *Eur. J. Med. Chem.* **2010**, *45*, 5286.
[7] F. Manetti, A. Santucci, G. A. Locatelli, G. Maga, A. Spreafico, T. Serchi, M. Orlandini, G. Bernardini, N. P. Caradonna, A. Spallarossa, *J. Med. Chem.* **2007**, *50*, 5579.
[8] Y. Y. Huang, L. Y. Wang, C. H. Chang, Y. H. Kuo, K. Kaneko, H. Takayama, M. Kimura, S. H. Juang, F. F. Wong, *Tetrahedron* **2012**, *68*, 9658.
[9] M. Maher, A. E. Kassab, A. F. Zaher, Z. Mahmoud, *J. Enzyme Inhib. Med. Chem.* **2019**, *34*, 532.
[10] K. Verschueren, M. Cobbaut, J. Demaerel, L. Saadah, A. R. D. Voet, J. V. Lint, W. M. de Borggraeve, *MedChemComm* **2017**, *8*, 640.
[11] J. C. Verheijen, D. J. Richard, K. Curran, J. Kaplan, M. Lefever, P. Nowak, D. J. Malwitz, N. Brooijmans, L. Toral-Barza, W.-G. Zhang, J. Lucas, I. Hollander, S. Ayral-Kaloustian, T. S. Mansour, K. Yu, A. Zask, *J. Med. Chem.* **2009**, *52*, 8010.
[12] P. Nowak, D. C. Cole, N. Brooijmans, M. G. Bursavich, K. J. Curran, J. W. Ellingboe, J. J. Gibbons, I. Hollander, Y. Hu, J. Kaplan, D. J. Malwitz, L. Toral-Barza, J. C. Verheijen, A. Zask, W. Zhang, K. Yu, *J. Med. Chem.* **2009**, *52*, 7081.
[13] E. Dreassi, A. T. Zizzari, M. Mori, I. Filippi, A. Belfiore, A. Naldini, F. Carraro, A. Santucci, S. Schenone, M. Botta, *Eur. J. Med. Chem.* **2010**, *45*, 5958.
[14] O. V. Dolomanov, L. J. Bourhis, R. J. Gildea, J. A. K. Howard, H. Puschmann, *J. Appl. Crystallogr.* **2009**, *22*, 339.
[15] G. M. Sheldrick, *Acta Crystallogr., Sect. A: Found. Crystallogr.* **2008**, *A64*, 112.
[16] G. K. Schwartz, M. A. Shah, *J. Clin. Oncol.* **2005**, *23*, 9408.
[17] N. P. Kumar, P. Sharma, T. S. Reddy, S. Nekkanti, N. Shankaraiah, G. Lalita, S. Sujanakumari, S. K. Bhargava, V. G. M. Naidu, A. Kamal, *Eur. J. Med. Chem.* **2017**, *127*, 305.
[18] A. Nagarsenkar, L. Guntuku, S. D. Guggilapu, K. Danthi Bai, S. Gannoju, V. G. M. Naidu, N. B. Bathini, *Eur. J. Med. Chem.* **2016**, *124*, 782.
[19] M. Kajstura, H. D. Halicka, J. Pryjma, Z. Darzynkiewicz, *Cytometry, Part A* **2007**, *71A*, 125.
[20] X. Huang, H. D. Halicka, F. Traganos, T. Tanaka, A. Kurose, Z. Darzynkiewicz, *Cell Prolif.* **2005**, *38*, 223.
[21] P. A. Leventis, S. Grinstein, *Annu. Rev. Biophys.* **2010**, *39*, 407.
[22] V. E. Kagan, J. P. Fabisiak, A. A. Shvedova, Y. Y. Tyurina, V. A. Tyurin, N. F. Schor, K. Kawai, *FEBS Lett.* **2000**, *477*, 1.

[23] H. van Genderen, H. Kenis, P. Lux, L. Ungethüm, C. Maassen, N. Deckers, J. Narula, L. Hofstra, C. Reutelingsperger, *Nat. Protoc.* **2006**, *1*, 363.
[24] S. H. Lee, X. W. Meng, K. S. Flatten, D. A. Loegering, S. H. Kaufmann, *Cell Death Differ.* **2013**, *20*, 64.
[25] L. A. Sena, N. S. Chandel, *Mol. Cell* **2012**, *48*, 158.
[26] S. Maharjan, M. Oku, M. Tsuda, J. Hoseki, Y. Sakai, *Sci. Rep.* **2014**, *4*, 1.
[27] A. Cossarizza, M. Baccaranicontri, G. Kalashnikova, C. Franceschi, *Biochem. Biophys. Res. Commun.* **1993**, *197*, 40.
[28] L. Galluzzi, N. Zamzami, T. de La Motte Rouge, C. Lemaire, C. Brenner, G. Kroemer, *Apoptosis* **2007**, *12*, 803.
[29] M. Redza-Dutordoir, D. A. Averill-Bates, *Biochim. Biophys. Acta* **2016**, *1863*, 2977.
[30] F. Sesti, O. E. Tsitsilonis, A. Kotsinas, I. P. Trougakos, *In Vivo* **2012**, *26*, 395.
[31] D. Trachootham, J. Alexandre, P. Huang, *Nat. Rev. Drug Discov.* **2009**, *8*, 579.
[32] Y. Zou, C. Yan, H. Zhang, J. Xu, D. Zhang, Z. Huang, Y. Zhang, *Eur. J. Med. Chem.* **2017**, *138*, 313.
[33] Y. Zheng, L. Zhu, L. Fan, W. Zhao, J. Wang, X. Hao, Y. Zhu, X. Hu, Y. Yuan, J. Shao, W. Wang, *Eur. J. Med. Chem.* **2017**, *125*, 902.
[34] J. M. Mates, F. M. Sanchez-Jimenez, *Int. J. Biochem. Cell Biol.* **2000**, *32*, 157.
[35] S. Kawanishi, Y. Hiraku, *Curr. Med. Chem. Anticancer Agents* **2004**, *4*, 415.
[36] H. Mizutani, S. Tada-Oikawa, Y. Hiraku, M. Kojima, S. Kawanishi, *Life Sci.* **2005**, *76*, 1439.

SUPPORTING INFORMATION

Additional supporting information may be found online in the Supporting Information section.

How to cite this article: Gaonkar S, Savanur MA, Nadaf AA, et al. Novel pyrazolo[3,4-*d*]pyrimidine derivatives inhibit human cancer cell proliferation and induce apoptosis by ROS generation. *Arch. Pharm.* 2020;e1900296.
https://doi.org/10.1002/ardp.201900296